

Evaluation of magnesium alloys for use as an intraluminal tracheal for pediatric applications in a rat tracheal bypass model

Sarah A. Luffy,^{1,2} Jingyao Wu,^{1,2} Prashant N. Kumta ,^{1,2,3,4,7} Thomas W. Gilbert^{1,2,5,6}

¹Department of Bioengineering, University of Pittsburgh, Pittsburgh, Pennsylvania, 15261

²McGowan Institute of Regenerative Medicine, University of Pittsburgh, Pittsburgh, Pennsylvania, 15261

³Department of Mechanical Engineering and Materials Science, University of Pittsburgh, Pittsburgh, Pennsylvania, 15261

⁴Department of Chemical and Petroleum Engineering, University of Pittsburgh, Pittsburgh, Pennsylvania, 15261

⁵Department of Cardiothoracic Surgery, Children's Hospital of Pittsburgh of UPMC, Pittsburgh, Pennsylvania

⁶ACell, Inc., Columbia, MD 21046

⁷Department of Oral Biology, School of Dental Medicine, University of Pittsburgh, Pittsburgh, Pennsylvania, 15261

Received 14 March 2018; revised 12 October 2018; accepted 17 October 2018

Published online 6 December 2018 in Wiley Online Library (wileyonlinelibrary.com). DOI: 10.1002/jbm.b.34277

Abstract: Tracheal stenting currently using non-degradable stents is commonplace for treatment of trauma, prolonged intubation related adult airway obstructions, and pediatric patients-associated tracheal stenosis conditions. Degradable tracheal stent placement will avoid complications of stent removal and restenosis. Widespread reports exist on degradable magnesium alloys success for orthopedic and cardiovascular applications but none to date for intra tracheal use. This research explores the use of pure Mg, AZ31, and Mg-3Y alloys for degradable tracheal stent assessment. *In vitro* evaluation of magnesium, prototype stents in a bioreactor simulate the airway environment and corrosion. Micro-CT imaging and biocompatibility evaluation helped assess the 24-week degradation of intraluminal alloy stents following implantation in a rat tracheal *in vivo* bypass model. Histological analysis indicate tissue response of the harvested stented trachea segments after each time point. Corrosion studies for each alloy indicate significant differences between

the simulated and control *in vitro* conditions. AZ31 exhibited the lowest volume loss of 6.8% in saline, while pure Mg displayed the lowest volume loss of 4.6% in simulated airway fluid (SAF), both at 1-week time points. Significant differences in percentage of total volume lost after 6 months were determined between the alloys over time. MgY alloy displayed the slowest corrosion losing only 15.1% volume after 24 weeks of immersion. Additionally, *in vitro* magnesium alloy corrosion was not significantly different from the percentage of total volume lost *in vivo* at 1-week time point. The study demonstrates promise of magnesium alloys for intraluminal tracheal stent application albeit viability of a clinically translatable model warrants further studies. © 2018 Wiley Periodicals, Inc. *J Biomed Mater Res Part B: Appl Biomater* 107B:1844–1853, 2019.

Key Words: magnesium alloy, biodegradable tracheal stent, tracheal obstruction

How to cite this article: Luffy SA, Wu J, Kumta PN, Gilbert TW. 2019. Evaluation of magnesium alloys for use as an intraluminal tracheal for pediatric applications in a rat tracheal bypass model. *J Biomed Mater Res Part B* 2019;107B:1844–1853.

INTRODUCTION

Tracheal obstructions are a rare clinical condition, especially among the pediatric patient population.¹ Tracheal obstructions are presented in both congenital and acquired instances. Congenital anatomical anomalies can result in airway obstruction, as in cases of tracheomalacia. Acquired tracheal obstructions are more common in children than congenital cases and are often the result of long-term intubation.^{2,3} Injury to the lumen of the trachea typically leads to the formation of scar tissue that can cause tracheal obstruction through a narrowing of the tracheal lumen. This condition is called tracheal stenosis.⁴ Severe cases of

tracheal obstruction resulting from acquired stenosis, often require multiple surgical and endoscopic procedures to achieve long-term goals of a desirable outcome.⁵ Pediatric tracheal stenosis is associated with severe morbidity and mortality, and the management of stenosis consistently presents challenges to clinicians.^{6,7}

Tracheal reconstruction is a primary treatment option for pediatric patients, however because of the small size of the pediatric airway, children do not experience the same success with resection and end-to-end anastomosis that adults can achieve.⁸ Ischemia and anastomotic tension resulting from reconstruction

Additional Supporting Information may be found in the online version of this article.

Sarah A. Luffy and Jingyao Wu contributed equally to this paper.

Correspondence: Prashant N. Kumta; e-mail: pkumta@pitt.edu or Thomas W. Gilbert; e-mail: thomasgilbert@acell.com

Contract grant sponsor: Division of Chemical, Bioengineering, Environmental, and Transport Systems; contract grant number: CBET-0933153

Contract grant sponsor: Division of Engineering Education and Centers; contract grant number: EEC-0812348

Contract grant sponsor: University of Pittsburgh

Contract grant sponsor: National Science Foundation

can cause restenosis. Slide tracheoplasty has become the treatment of choice when surgery is necessary. While alternative temporary or definitive methods are being developed for those who are not surgical candidates, surgical reconstruction is still considered the ideal approach for management of tracheal stenosis.⁹ Endoscopic management of tracheal stenosis by balloon dilation is used as a method of treatment when attempting to avoid open surgical procedures in both children and adults.¹⁰ However, the effects of balloon dilation on the stenotic trachea are poorly understood, and repeated treatments are often necessary. In order to avoid a recurrence of tracheal stenosis following surgical repair, tracheal stents have been used with reasonable success. Minimally invasive deployment options for intraluminal balloon expandable stents have become an attractive option for the treatment of tracheal stenosis. Complications associated with tracheal stenting include encapsulation and incorporation into the mucosal tissue, migration, perforation, and compromised mucociliary clearance of the airway.¹¹

Currently available tracheal stents vary in material composition and physical geometry, as well as application purpose. Stent selection typically depends on whether the patient has a benign or malignant disease, the need for the stent is temporary or permanent, the physician's experience with stent insertion, and finally, the overall cost of the procedure itself.¹² Silicone tubes,¹² self-expanding metallic stents,¹³ and balloon expandable stents⁴ are the most common options for tracheal stents. However, the permanent existence of the stent and the difficulty of the stent removal result in severe clinical issues when using the currently available commercial tracheal stents.^{9,11,12}

The history of magnesium particularly over the last few years has demonstrated its potential for use as a degradable biomaterial. Magnesium is also known to have strong biocompatibility due to its naturally occurring presence in the human body.¹⁴ Since magnesium can experience fast degradation and loss of mechanical properties, it is alloyed with other elements, such as aluminum,^{15,16} yttrium,¹⁷ calcium,^{18,19} zinc²⁰ and other rare earth elements,²¹ to increase the aqueous corrosion resistance and hence, decrease the rate of degradation. Magnesium alloys degrade in aqueous environments and are resorbed by the body through oxidation making them attractive materials

for the development of a degradable tracheal stent. Our previous study has demonstrated that the body could tolerate the presence of an Mg-3Y extraluminal stent with a mild host response, without negatively impacting the native cartilage after 8 weeks.²² However, the performance of magnesium alloys within the trachea remains unknown. Standard *in vitro* corrosion assays inaccurately predict the *in vivo* behavior of magnesium alloys.²³ Furthermore, the response of the tracheal tissue to the presence of magnesium cannot be predicted without adequate models.

The objective of this research is to evaluate the degradation behavior of three magnesium alloy based prototype tracheal stents, namely Mg-3Y, AZ31, and 99.9% pure Mg, in a simulated *in vitro* airway environment. Additionally, the *in vivo* degradation and biocompatibility of the prototype intraluminal stents were further evaluated in a specially developed rat tracheal bypass model. The *in vitro* results were then compared to the degradation kinetics *in vivo* to determine a correlation between the degradation of magnesium alloys in the airway.

MATERIALS AND METHODS

Stent fabrication and characterization

Commercially available 99.9% pure magnesium and AZ31 alloy were obtained from Goodfellow (Coraopolis, PA). Magnesium alloy containing 3 wt % Y (Mg-3Y) was obtained from Helmholtz Zentrum Geesthacht Institute of Materials Research, Geesthacht, Germany, which was kindly provided as a gift from Dr. Norbert Hort and Dr. Frank Witte. All the three materials were T4 heat treated at 525 °C under a protective environment of Ar + 0.1% SF₆ for 8 h to homogenize the intermetallics and the various alloying elements present in the alloy matrix. The magnesium alloys were then machined into stents at the University of Pittsburgh Swanson School for Product Innovation (SCPI), with an outer diameter of 2.25 mm, inner diameter of 1.25 mm and length of 5 mm (Figure 1(A)).

To remove the stresses imparted by the machining process, the stents were then subjected to a second heat treatment at 205°C for 1.5 h in ultra-high purity argon (UHP-Ar). All the stents were sonicated in isopropanol for 5 min and dried in air three times, and then terminally sterilized with 2MRad γ -irradiation.

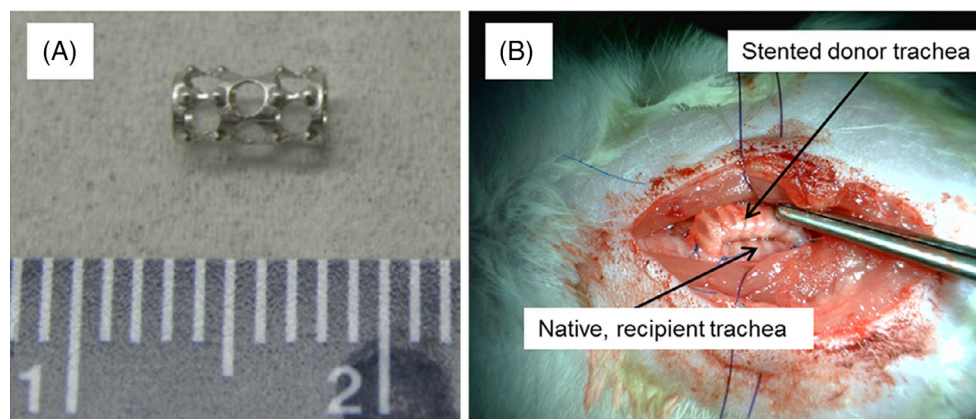


FIGURE 1. (A) Magnesium intraluminal tracheal stent; (B) surgical placement of an intraluminal tracheal stent in a Lewis rat tracheal bypass model.

TABLE I. The Chemical Composition of SAF Medium

Component	g/L
Magnesium chloride	0.095
Sodium chloride	6.019
Potassium chloride	0.298
Disodium hydrogen phosphate	0.126
Sodium sulfate	0.063
Calcium chloride dihydrate	0.368
Sodium acetate	0.574
Sodium hydrogen carbonate	2.604
Sodium citrate dihydrate	0.097
Porcine stomach mucin	0.6

***In vitro* evaluation of magnesium stent**

Bioreactor simulation of *in vitro* degradation. *In vitro* degradation of magnesium tracheal stents was assessed using a bioreactor system. The stent was placed in a decellularized Lewis rat trachea and mounted in a bioreactor chamber containing extraluminal media and intraluminal media. Polycarbonate square chambers held the stented trachea on hollow steel rods that allowed for internal media flow through the trachea and pump tubing. Side ports on the chambers allowed for samples to be taken from the external media of the chamber to measure the amount of magnesium present in the media.

The three stent alloys were evaluated in both simulated airway fluid (SAF) media as described by Marques et al.²⁴ and 0.9% saline (Fisher Scientific, Hampton, NH) for a control comparison. The composition of the SAF is listed in Table I. A total of $n = 3$ stents were used for each alloy and each condition. The stented decellularized trachea persisted in the bioreactor chamber for 1 week. A continuous flow pump (Ismatec) was used to circulate media at a constant rate of 0.5 mL/h for the duration of the experiment.

ICP analysis. Samples of the media (0.5 mL) were taken at 1, 3, 5, and 7 days *in vitro*. *In vitro* degradation kinetics were assessed using inductively coupled plasma optical emission spectroscopy (ICP-OES, iCAP duo 6500 Thermo Fisher, Waltham, MA). Standard calibrations were made to achieve the baseline magnesium concentrations in parts per million (ppm). Every sample taken from the bioreactor with SAF conditions was diluted 1:20 in saline, and by diluting only SAF in saline by 1:20, a blank was also created. The blank was used to subtract the mucins and salts found in SAF and gain a more accurate measurement of the magnesium dissolved from the stent at each time point. Each sample taken from the bioreactor with control conditions was also diluted 1:20 in fresh saline, and a saline blank was created.

Upon completion of ICP, the SAF and saline blanks were subtracted from the SAF and control measurements, respectively. The difference was then multiplied by 20 to achieve the amount of magnesium measured in the media at 1, 3, 5, and 7 days, respectively *in vitro* for both the simulated and control conditions for each of the considered magnesium stent.

Micro-CT analysis. After 1 week of *in vitro* testing, the stents were imaged using micro-CT and processed for quantification

of the volume loss. The stents were manually removed from the bioreactor chambers and gently removed from the decellularized trachea before being subjected to micro-CT imaging. The 2-D dicom files of the *in vitro* stents were then processed using the Mimics software. Three-dimensional volumes of the stents were generated for each of the alloys tested *in vitro* for 1 week and compared to the 3-D volumes of the original stents prior to undergoing testing. The difference in volume was calculated and an overall percent of volume lost over time was quantified. Statistical analysis was performed to determine the significant differences between the original stent volume and the stent volume at each endpoint for each alloy used in this study.

***In vivo* evaluation of tracheal stent**

Surgical procedure. Donor female Lewis rats were anesthetized by intraperitoneal injection of ketamine (80 mg/kg) xylazine (8 mg/kg) to maintain the surgical plane of anesthesia, and were euthanized via exsanguination. The tracheas were harvested to provide a bypass surgical model for stent evaluation, Figure 1(B). Recipient animals were anesthetized in a similar way. Aseptic technique was used to expose the proximal cervical trachea through a midline neck incision. Small proximal and distal defects separated by five cartilage rings were created in the recipient trachea. The stent was placed intraluminally in the donor trachea, which was anastomosed to the distal and then proximal defects using 7-0 prolene suture (Ethicon, Somerville, NJ). The bypass model allowed for airway communication and evaluation of the non-optimized stent geometries *in vivo* without compromising respiration. The skin incision was closed using an interrupted suturing technique with 5-0 PDS suture (Ethicon, Somerville, NJ). Proper anastomosis was determined by visual inspection and by the absence of any sub-cutaneous air upon closure.

All the animals were recovered from anesthesia and monitored until alert and active. In the immediate post-operative period, buprenorphine hydrochloride (0.05 mg/kg, Butler Schein) was administered every 12 h for 5 days for pain management.

Micro-CT analysis. Using micro-CT (Inveon, Siemens, Munich, Germany), the magnesium stents were imaged prior to implantation. Upon harvesting the trachea-stent complex, the tissue was fixed in formalin and subjected to the same micro-CT imaging. The two-dimensional Dicom files were processed using the Mimics software (Materialize, Mimics 12.01, Belgium). Three-dimensional volumes of the stents were generated for the data prior to implantation and at 1-, 8-, 16-, and 24-week explants. The difference in volume (mm^3) was calculated and an overall percent of total volume lost over time was quantified. The total volume loss served as an indication of the corrosion behavior of the stent *in vivo*. Statistical analysis was performed to determine the significant differences between original stent volume and stent volume at each endpoint for each alloy in this study. Data from the *in vivo* and *in vitro* stent degradation were compared and analyzed for statistical significance as well. Statistical analysis were

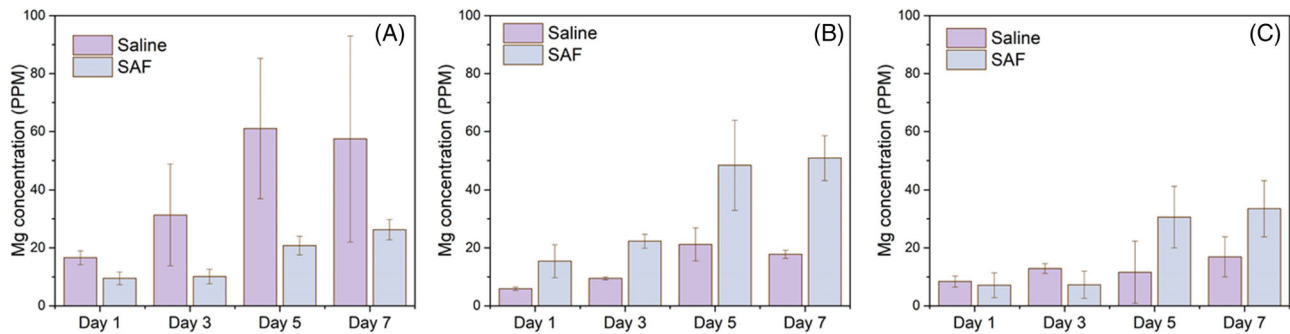


FIGURE 2. Average magnesium concentrations released from magnesium tracheal stents at 1, 3, 5, and 7 days *in vitro* for both SAF and saline conditions (A) pure Mg, (B) AZ31 alloy, (C) Mg-3Y alloy.

performed following the protocol given in the statistical analysis section below.

Histological evaluation. The stented trachea bypass complex was harvested and fixed in 10% neutral buffered formalin (NBF), dehydrated, and embedded in paraffin for histological analysis. Cross-sectional tissue specimens were cut along the longitudinal axis of the trachea-stent bypass in 5-micron sections. Following deparaffinization and rehydration, sections of the trachea-stent complex were stained with Hematoxylin and Eosin (H&E).

Statistical analysis

All statistical analyses were performed using the SPSS package (version 20.0; IBM SPSS, Inc., Chicago, IL). Statistical significance was set at $p < 0.05$. To compare the differences of corrosion within and between the alloy groups over time, a two-way independent ANOVA with Tukey's post hoc analysis was used to analyze the percent of total stent volume lost for each stent. Percent of total stent volume lost over time is reported as the mean standard deviation.

RESULTS

In vitro degradation of tracheal stent in bioreactor

Magnesium concentration measured from the pure Mg stent in saline control media was 16.6 ± 2.4 ppm at day 1. The magnesium concentration nearly doubled by day 3 (31.3 ± 17.5 ppm), peaked at day 5 (61.1 ± 24.1 ppm), and then slightly decreased by day 7 (57.5 ± 35.5 ppm). ICP-OES measured the presence of the greatest amount of magnesium from the pure Mg among all alloys in saline control media at day 5 *in vitro* (61.1 ± 24.1 ppm) (Figure 2(A)). Less magnesium was measured throughout in SAF conditions for the pure Mg stent compared to the saline control. An increasing trend was observed in magnesium concentration collected from SAF *in vitro* at day 1 (9.5 ± 2.2 ppm) to SAF *in vitro* at day 7. Magnesium concentration for SAF *in vitro* on day 3 was 10.1 ± 2.5 ppm. After 5 days in SAF, the magnesium concentration was measured by ICP to be 20.8 ± 3.2 ppm. Peak concentration of magnesium for the pure Mg stent in SAF media was measured on day 7 to be 26.3 ± 3.5 ppm.

Magnesium measurements from AZ31 stents using ICP-OES resulted in greater concentrations of magnesium under SAF conditions than under saline control conditions (Figure 2(B)). At saline control *in vitro* on day 1, magnesium concentration

was 5.9 ± 0.6 ppm. *In vitro* on day 3, AZ31 magnesium concentration steadily increased to 9.5 ± 0.5 ppm, and continued to increase to a peak saline control concentration for AZ31 of 21.2 ± 5.7 ppm by day 5. By day 7, the magnesium concentration had decreased to 17.8 ± 1.4 ppm. Magnesium concentrations for AZ31 stents in SAF however, showed a steady increase from *in vitro* on day 1 to day 7. ICP-OES measured magnesium concentrations in SAF at 15.4 ± 5.7 ppm at day 1. Day 3 the magnesium concentration was measured at 22.3 ± 2.4 ppm. The increasing trend continued at SAF *in vitro* on day 5 (48.4 ± 15.5 ppm) peaking at day 7 (50.9 ± 7.7 ppm).

For the Mg-3Y stents in the saline control conditions, the magnesium concentrations steadily trended upward from *in vitro* day 1 to *in vitro* day 7 (Figure 2(C)). ICP-OES measured a magnesium concentration for Mg-3Y in saline on day 1 at 8.4 ± 1.9 ppm, and increased to 12.9 ± 1.7 ppm at day 3. By *in vitro* day 5, the magnesium concentration for the saline control conditions for Mg-3Y slightly decreased to 11.6 ± 10.7 ppm, before increasing to 16.9 ± 6.9 ppm by day 7. Greater magnesium concentration was measured from the SAF conditions for the Mg-3Y stents *in vitro*. No steady, increasing trend for the SAF conditions for Mg-3Y stents was however, observed. ICP-OES measurements resulted in similar day 1 and day 3 magnesium concentration results (7.1 ± 4.3 ppm and 7.3 ± 4.7 ppm), respectively and increased but similar measurements were observed at day 5 and day 7 (30.6 ± 10.6 ppm and 33.5 ± 9.7 ppm).

After the stents were tested for 1 week *in vitro* under both SAF and control saline conditions, micro-CT images were obtained (Figure 3) and the volume loss was accordingly calculated (Figure 4). The percentage of total volume lost for pure Mg stent after 1 week *in vitro* under SAF conditions was $4.55 \pm 8.67\%$. Saline control conditions for 1 week *in vitro* however, resulted in $21.81 \pm 16.98\%$ total stent volume lost. For AZ31 alloy on the other hand, greater total stent volume loss was observed after 1 week under SAF *in vitro* conditions with $12.24 \pm 8.43\%$ total stent volume lost. This result was approximately double the results of $6.82 \pm 9.12\%$ total stent volume lost after 1 week *in vitro* under control saline conditions. In the case of Mg-3Y stents, similar to pure Mg, the results from 1 week *in vitro* demonstrated greater volume loss under saline control conditions with $15.22 \pm 1.99\%$ total volume lost. The Mg-3Y stents under SAF conditions however,

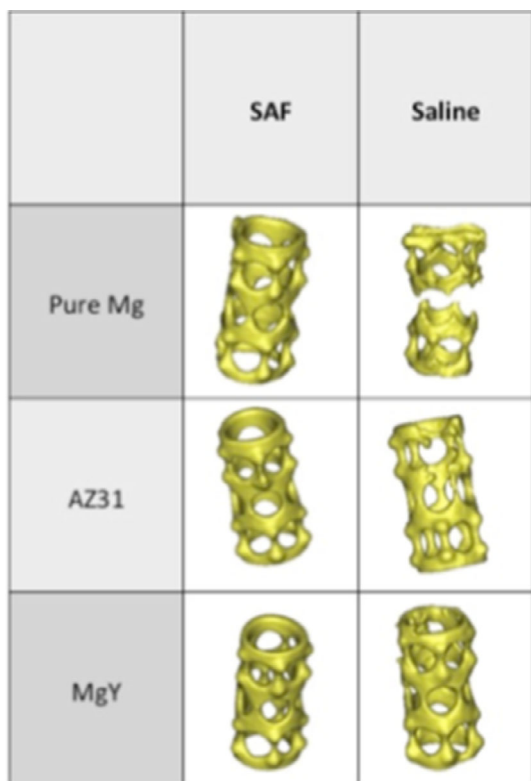


FIGURE 3. Representative three-dimensional micro-CT images of pure Mg, AZ31, and Mg-3Y stents after 1 week of *in vitro* testing in SAF media and saline control conditions.

for 1 week *in vitro* experienced only $9.46 \pm 4.95\%$ total stent volume lost.

The statistical analysis showed that significant differences in ICP-OES results were observed between the magnesium stents under SAF conditions ($p = 0.019$), while no significant differences between magnesium stents were observed for the saline control conditions ($p = 0.224$). Magnesium content measured from AZ31 and Mg-3Y stents were not significantly different under SAF conditions, however the magnesium content measured for pure Mg under SAF conditions was significantly different from AZ31 ($p = 0.035$) and Mg-3Y ($p = 0.029$). No significant differences in magnesium concentration were observed between any of the magnesium stents under saline control conditions. When comparing the 1-, 3-, 5-, and 7-day time points under SAF conditions, no significant differences between magnesium stents were observed ($p = 0.478$). Under saline control conditions, however, significant differences were observed between magnesium stents over time ($p = 0.031$), but no significant differences were found among ICP-OES results at 1, 3, 5, and 7 days. The micro-CT data indicated that significant differences were observed between all alloys under the saline *in vitro* control conditions, while only pure Mg experienced significantly different results under SAF *in vitro* conditions.

ICP-OES allowed for the measurement of magnesium concentration in media every 48 h throughout 1 week. The measurement of magnesium in the media is representative of the amount of magnesium lost from the stent. Measurements from

ICP-OES revealed that the most magnesium was lost on day 5 of the pure Mg in saline control media. Pure Mg stents also experienced the greatest volume lost among the three stents under saline control conditions after 1 week *in vitro*. The AZ31 alloy experienced the most magnesium loss on *in vitro* day 7 under SAF conditions. This is also consistent with the greatest amount of stent volume lost according to the micro-CT analysis among all the alloys considered under SAF conditions after 1 week *in vitro*.

***In vivo* degradation of tracheal stent in the rat trachea bypass model**

All the animals tolerated the tracheal bypass surgery well and survived to their preassigned end point. No abnormal behavior was observed that could have been related to the presence of a resorbable stent structure. The volume loss of the magnesium stents was calculated based on the micro-CT data (Figure 5). Pure Mg showed a volume loss at 1 week of $6.3 \pm 1.6\%$. At 8 weeks, the volume loss was $34.1 \pm 15.7\%$, which was not a significant increase in mass loss compared to 1 week. The volume loss continued to increase through 16 weeks to $65.9 \pm 7.9\%$, a significant increase from the 1- and 8-week time points. Pure Mg also showed the greatest volume loss of the three alloys tested at 16 weeks. After 24 weeks, the observed volume loss of $64.2 \pm 16.8\%$ was similar to the 16 weeks results. Representative 3D structures of the pure Mg stent at each time point are also illustrated in Figure 6(A). The structure of the stent was preserved after 1 week, but after 8 weeks stent fracture and significant volume loss had occurred. By 16 and 24 weeks, in fact, the stent structure was completely compromised and only fragments of the metallic material remained.

Corrosion of the AZ31 stent did not appear to follow any discernable trend or pattern. Total stent volume lost after 1 week was $28.2 \pm 16.4\%$. Corrosion appeared to decrease after 8 weeks with a volume loss of only $13.85 \pm 11.1\%$.

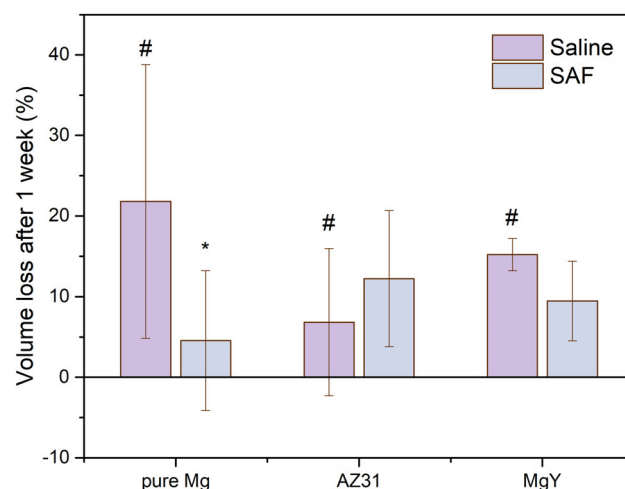


FIGURE 4. Percent of total volume lost during *in vitro* testing for each alloy after 1 week in saline or 1 week in SAF. The (#) indicates significant differences were observed between all alloys under the saline *in vitro* control conditions, while the (*) indicates only pure Mg experienced significantly different results under SAF *in vitro* conditions.

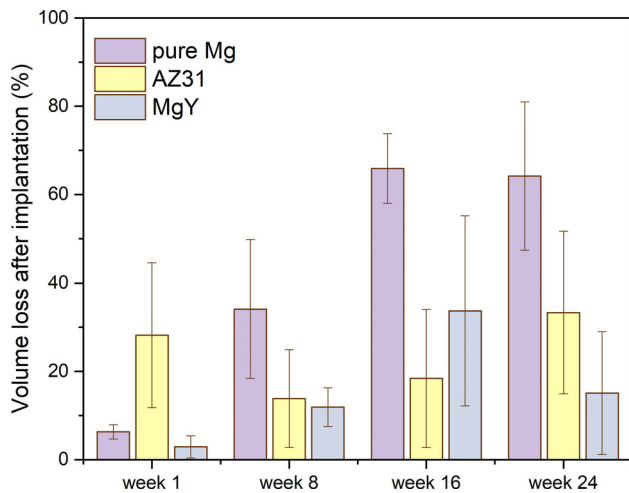


FIGURE 5. Percent of total volume lost during *in vivo* testing for each alloy at 1, 8, 16, and 24 weeks.

After 16 weeks, the total AZ31 stent volume loss increased to $18.4 \pm 15.62\%$, and continued to a maximum stent volume loss of $33.3 \pm 18.4\%$ after 24 weeks. These findings are not consistent with the morphology of the stent as depicted by the 3D constructed micro-CT images in Figure 6(B). No corrosion is evident after 1 week, but the structure began to change at 8 weeks. By 16 weeks, the stent structure is compromised by corrosion and fracture, which continued at the 24-week time point. The variability among AZ31 stent volume loss was so large that no consistent patterns in corrosion were observed.

Mg-3Y stents on the other hand, experienced the least amount of stent volume lost among all the alloys considered at 1 week *in vivo* with $2.9 \pm 2.5\%$. The total stent volume lost showed a continuous increase to $11.9 \pm 4.4\%$ after 8 weeks and $33.7 \pm 21.5\%$ after 16 weeks, before decreasing to $15.1 \pm 13.9\%$ after 24 weeks. This corrosion behavior is similar to that of the pure Mg stents - a continuous increase in volume loss from 1-week to a peak at 16 weeks, before slightly decreasing after 24 weeks. Although the corrosion patterns are similar to the pure Mg stents, significant differences were observed between Mg-3Y and pure Mg for total stent volume lost. Representative corrosion patterns of the Mg-3Y stents at each time point are illustrated in Figure 6 (C). The collected images reveal an intact stent at 1-week, with progressive corrosion and fracture beginning at 8 weeks. By 24 weeks, the Mg-3Y stents appear completely compromised with a globular morphology.

Statistical analysis indicated significantly more stent corrosion for pure Mg than for AZ31 and Mg-3Y ($p = 0.003$), while no significant differences were observed in stent corrosion between the magnesium alloys AZ31 and Mg-3Y ($p = 0.376$). Post-hoc analysis showed that Mg-3Y corroded the least at the 1-week time point. Pure Mg alloys showed the most corrosion with the greatest amount of total volume lost at the 16-week time point.

Corrosion results compared at early time points of 1 and 8 weeks did not have significant differences ($p = 0.633$), while the same is true for results compared at late time points of 16 and 24 weeks ($p = 0.999$). Significant differences in stent

corrosion were observed between the 1-week and both the 16- and 24-week time points ($p = 0.002$). Comparisons of the 8-week time point with both the 16- and 24-week time points revealed significant differences in stent corrosion ($p = 0.030$ and $p = 0.034$, respectively). Even with differences in stent corrosion at the 1-week time point, the structure of the stents remained intact. Changes in stent structure began to occur by 8 weeks for all the alloys with major corrosion occurring at the thinner areas of the stent. Stent fractures putatively lead to a compromise of the structure of the stent, usually occurring at the later time points. It is unclear whether the fractures result from corrosion or mechanical stresses, and the results indeed vary among alloys and time points.

Histologic response to magnesium tracheal stent in rat bypass model

After 1 week *in vivo*, H&E staining showed the presence of a normal looking epithelium without any ciliated cells noticeably present in the stented airway (Figure 7(A, B)). There was also a prominent mononuclear cell response. Fibrous tissue appeared to surround the perimeter of the stent after 1 week, but there was no evidence of any stent encapsulation. At 8 weeks, the mononuclear cell population had decreased (Figure 7(C, D)). Although there was still some hypercellularity present after 8 weeks *in vivo*, the epithelium of the stented airway appeared healthy with noticeable secretory and ciliated cells. Evidence of stent encapsulation was present after 16 weeks with clear visualization of growth around the stent (Figure 7(E, F)). Also, the presence of a ciliated epithelium was maintained. The encapsulated portions of the stent showed a morphology that was less organized at 24 weeks, suggesting collapse of the structure (Figure 7(G, H)). Although a ciliated epithelium remained in particular areas, the epithelium generally appeared more squamous in nature. The areas of growth around the stent and throughout the graft contained evidence of vascularization as indicated by the presence of red blood cells. Airway communication between the native airway and stented graft remained even after 24 weeks.

One week after AZ31 stent placement *in vivo*, H&E staining of the stented trachea revealed a squamous epithelium with a large presence of mononuclear cells (Figure 8(A, B)). At the 8-week time point, histology revealed both columnar and squamous epithelium with some stent encapsulation and cell growth (Figure 8(C, D)). The columnar epithelium had progressed to a ciliated epithelium after 16 weeks, with reduced presence of mononuclear cell response (Figure 8(E, F)). After 24 weeks, an open lumen was maintained with the presence of ciliated cells (Figure 8(G, H)). Overall, a columnar ciliated epithelium with secretory cells, a mononuclear cell population with no evidence of a foreign body response, and vascularity of the graft by evidence of red blood cells was observed.

Mg-3Y histology revealed mononuclear cells and hypercellularity around the stented graft after 1 week *in vivo* (Figure 9(A, B)). Some areas of the epithelium appeared normal, while squamous epithelium was observed in areas of contact with the stent. Mg-3Y was the only alloy to reveal a potential indication of foreign body response with a limited number of giant cells present after 1 week. By 8 weeks, an

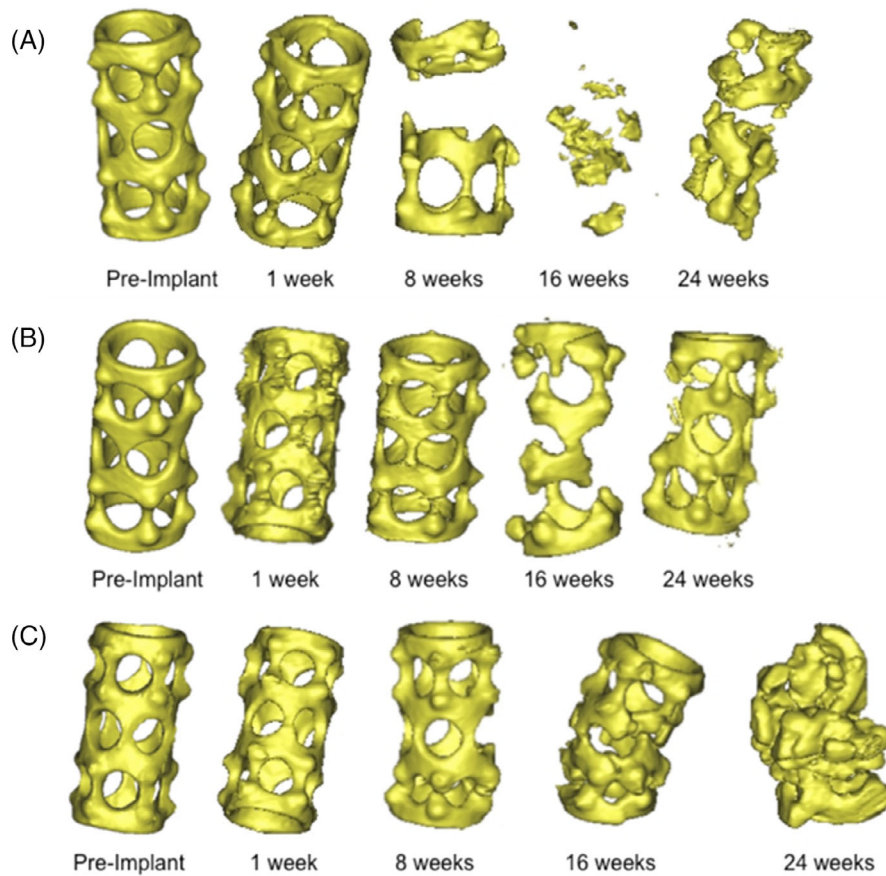


FIGURE 6. Representative images of three-dimensional micro-CT volumes for magnesium stents prior to implantation and at the 1-, 8-, 16-, and 24-week time points (A) pure Mg, (B) AZ31 alloy, (C) Mg-3Y alloy.

open lumen with a normal epithelium was observed with growth and encapsulation around the stent (Figure 9(C, D)). After 16 weeks *in vivo*, a prominent inflammatory response was observed in one animal that appeared to surround the graft with evidence of a foreign body response revealed by the presence of neutrophilic cells and multinucleated giant cells (Figure 9(E, F)). A mucous plug was observed in the

lumen of one graft, possibly indicating an immune response even after 24 weeks (Figure 9(G, H)).

In general, histology revealed similar results among all three magnesium stents. Airway communication between the stented graft and the native airway was maintained throughout the study with the tracheal bypass model. A ciliated epithelium was present after 8 weeks and persisted

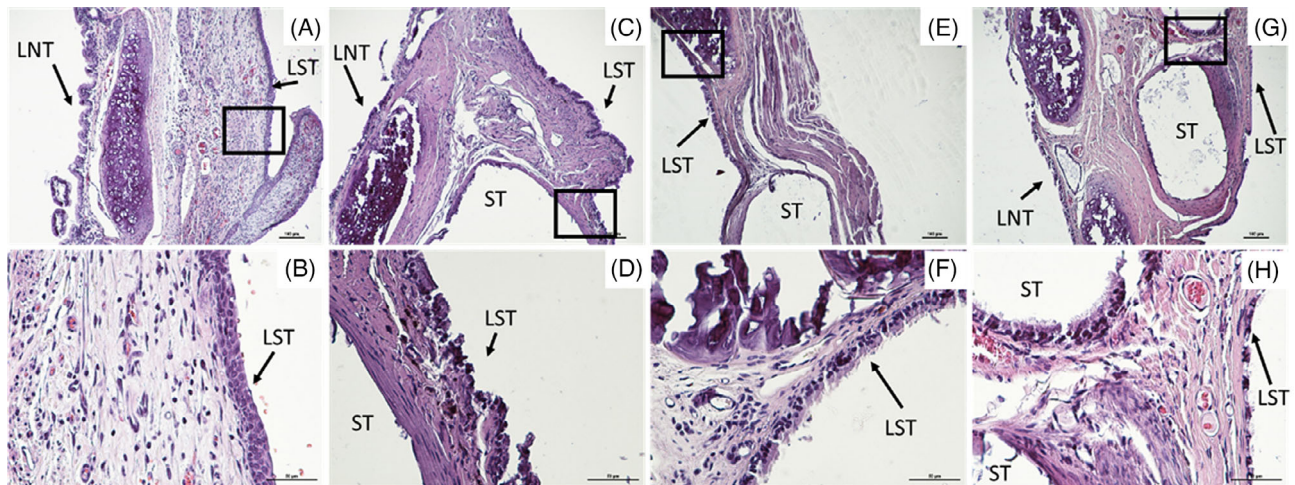


FIGURE 7. Representative histology (H&E) from Pure Mg stents *in vivo* at (A, B) 1 week, (C, D) 8 weeks, (E, F) 16 weeks, and (G, H) 24 weeks. LNT: lumen of native trachea, LST: lumen of stented trachea, ST: stent. Error bar: 100 μ m for (A), (C), (E) and (G); 50 μ m for (B), (D), (F), and (H).

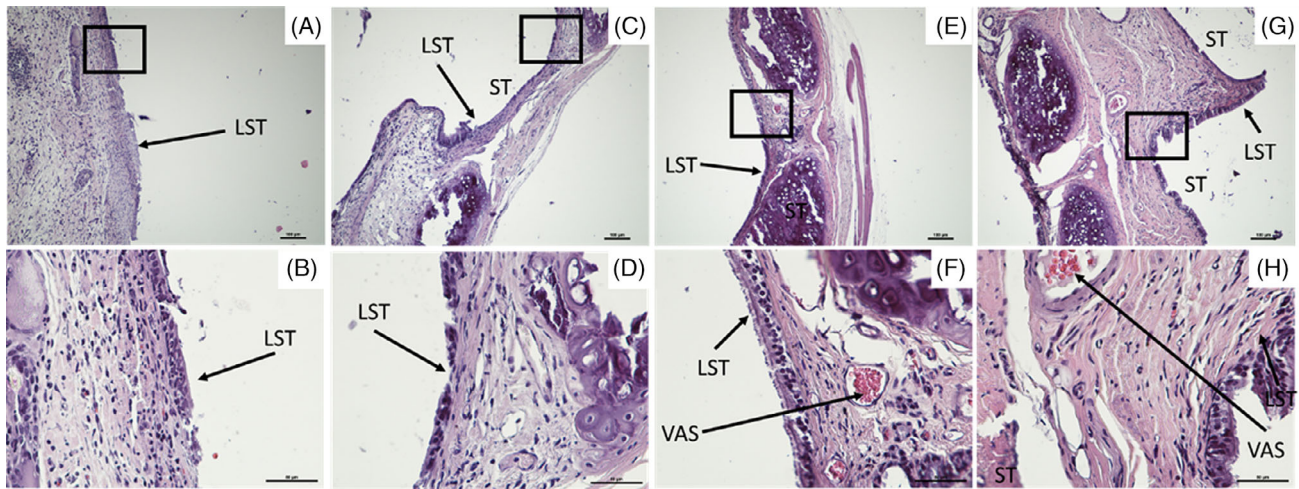


FIGURE 8. Representative histology (H&E) from AZ31 stents *in vivo* at (A, B) 1 week, (C, D) 8 weeks, (E, F) 16 weeks, and (G, H) 24 weeks. LNT: lumen of native trachea, LST: lumen of stented trachea, ST: stent, VAS: vascularization. Error bar: 100 μm for (A), (C), (E), and (G); 50 μm for (B), (D), (F), and (H).

until 24 weeks. The Mg-3Y stents were the only stents to indicate a slight inflammatory or foreign body response. All alloys experienced tissue growth around the stent leading to encapsulation around 16 weeks and increasing by 24 weeks. At the 24-week time point, the stented graft was vascularized by the native trachea as demonstrated by the presence of red blood cells.

DISCUSSION

Results from ICP and Micro-CT demonstrated that pure Mg stents registered the highest amount of magnesium measured and volume loss *in vitro*, and experienced the greatest volume lost *in vivo*. Micro-CT results also revealed the closest correlation between magnesium stent volume lost at 1 week *in vivo* and after 1 week *in vitro* under SAF conditions. Differences between the *in vitro* results of saline control conditions and the *in vivo* results from 1 week, as compared to the SAF *in vitro* results, suggest the SAF media is contributing to creating an environment *in vitro* that is more closely related to an *in vivo* airway environment. Because the bioreactors used to evaluate the magnesium stents *in vitro* were continuous flow, the varying pressures associated with normal respiration were not applied to the stents *in vitro*. The tracheal bypass model also places the stented airway in a partially passive trachea environment. As a result, the continuous flow system may be a good model for comparing *in vitro* results to the *in vivo* bypass model. Similarities nevertheless, between the *in vitro* and *in vivo* results are very encouraging for the evaluation of magnesium alloys. Historically, *in vitro* evaluation of magnesium could not be relied upon to accurately predict the *in vivo* behavior.²⁵ To further address the limitations of the *in vitro* study, magnesium alloys should be evaluated at later time points *in vitro* and compared to later time points *in vivo* as well.

All three of the magnesium stents experienced greater correlation between volume loss after 1 week *in vivo* and volume loss after 1 week *in vitro* under SAF conditions. These results suggest the simulated conditions are more accurately predicting the behavior of magnesium stents after 1 week *in vivo*.

Little is known about the effects of magnesium on the airway, and evidence of a normal and functional airway epithelium following magnesium stent placement are certainly encouraging results. Since this study was limited by employing preliminary prototype magnesium stents with a geometry that was not optimized, the tracheal bypass model was therefore used for tracheal stent evaluation as part of an initial pilot study. It is clearly unknown whether similar results could be achieved without the bypass model and using a more optimized stent geometry that would be traditionally used for tracheal stent applications. It would also be interesting to compare these alloys in an *in vivo* study using a standard tracheal bypass model, but putting in place the stent in the actual native trachea while allowing for the donor trachea to truly bypass the stented native airway. Because of limitations in achieving a machineable and appropriately sized rat tracheal stent, we did not attempt to explore and study this alternative surgical model.

Mild evidence of a foreign body response to the Mg-3Y stents was observed *in vivo* with the isolated presence of a possible foreign body giant cell after 1 week and hypercellularity with neutrophils and multinucleated giant cells after 16 and 24 weeks. Neither AZ31 nor pure Mg stents showed however, any signs of chronic, foreign body response throughout the *in vivo* study. Histological analysis of all the stents revealed the presence of a normal, ciliated epithelium in the stented airway by 8 weeks and persisting after 24 weeks. Although present, the epithelium of the stented airway appeared more squamous in nature by the 24 weeks' time point. After 1 week *in vivo*, the stented airway also appeared squamous in some areas, but this may have been the result of surgical manipulation since it takes time for the graft to become revascularized after transplantation. By 8 weeks, a ciliated epithelium was observed for all the stents. Encapsulation of the stents began between the 8 and 16-week time points.

Micro-CT imaging provided insights into the corrosion patterns of the magnesium stents over time. By 16 or even 8 weeks, all the stents appeared compromised with total stent

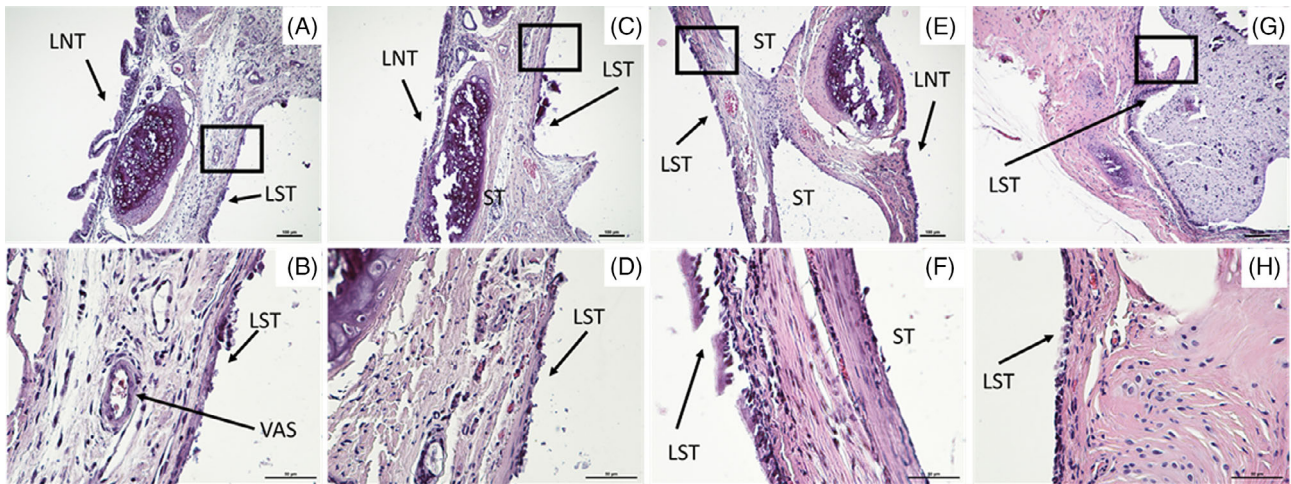


FIGURE 9. Representative histology (H&E) from Mg-3Y stents *in vivo* at (A, B) 1 week, (C, D) 8 weeks, (E, F) 16 weeks, and (G, H) 24 weeks. LNT: lumen of native trachea, LST: lumen of stented trachea, ST: stent, VAS: vascularization. Error bar: 100 μ m for (A), (C), (E), and (G); 50 μ m for (B), (D), (F), and (H).

volume losses between 18% and 66% after 16 weeks. As expected, the pure Mg stent did experience greater corrosion *in vivo* than the magnesium alloys. Mg-3Y and AZ31 both experienced a maximum of 33% total stent volume lost, while Mg-3Y peaked after 16 weeks and AZ31 did not reach maximum volume loss until 24 weeks. Visually, the compromised structure of the Mg-3Y stents can be qualitatively observed as more compromised than that of the AZ31stent, even though the stents experienced similar amounts of total volume lost. This could be the result of the alloy composition or the stresses experienced by the stents *in vivo*. Statistical analysis also supported that the differences in volume lost which were observed between the early and late time points are indicative of a possible pattern being followed affecting the rate of degradation. The volume loss calculated in Figure 5 showed large sample-to-sample variation attributed to the following two reasons. First, the relatively low number of samples. Due to the high cost of stent fabrication, we used only three stents for each group. Second, the complexities involved in the fabrication process itself. There are too many variables involved in processing of the stents. These include inhomogeneity in the alloy, machining related variation introduced in the alloy microstructure, heat treatment conditions causing changes in the microstructure, compositional homogeneity etc. These will likely lead to variations in the stent chemical composition, stent size, and surface condition which are all key factors affecting the local and bulk overall corrosion of magnesium. We believe that if we optimize the stent manufacturing process and increase the samples size, we will be able to reduce the variability seen in the results.

An important limitation of the *in vivo* study however, is that the tracheal stent intended for treatment of tracheal stenosis was applied to a normal, healthy trachea in a bypass model. Because the stent geometry was not yet optimized and little is known about the use of magnesium in the trachea itself, this study is actually aimed to evaluate the effects of magnesium on the airway environment. Histological

analysis demonstrated minimal effects of magnesium on the function of the airway environment at early time points (1 week) and up to 24 weeks. Another study evaluating the effects of magnesium on the trachea at later time points of 6 months to 1 year, could provide further understanding on the longer-term effects of magnesium on the airway environment.

Further additional *in vitro* and *in vivo* testing of magnesium alloys as tracheal stents are clearly therefore, necessary to predict and understand the degradation processes of the magnesium alloy and magnesium alloy based stent. The results of this study nevertheless, show preliminary evidence supporting further investigation that is needed for use of magnesium alloys as a potential material for a degradable tracheal stent for pediatric patients. These studies are being planned for the near future.

CONCLUSIONS

Tracheal stents successfully manage adult airway obstructions, including tracheal stenosis, but are used primarily as a treatment option of last resort for pediatric patients because of their permanent nature. A degradable tracheal stent would provide pediatric patients the opportunity for growth potential while maintaining an open lumen. The magnesium alloys evaluated in this preliminary pilot study demonstrate potential for their use in the tracheal environment. Initial *in vitro* studies using SAF provide support for additional *in vitro* testing to more closely mimic the response of magnesium alloy stents *in vivo*. This study also illustrates the trachea's tolerance and acceptance of magnesium after 6 months with minimal foreign body response and without any negative effects on airway function. More studies, however, will be necessary to further develop the stent design and alloy composition followed by further optimization of the mechanical properties in order to support a pediatric airway with tracheal stenosis. These studies are planned for the future.

ACKNOWLEDGMENTS

The authors gratefully acknowledge the support of the NSF funded Engineering Research Center-Revolutionizing Metallic Biomaterials (RMB) through grant-EEC-0812348. PNK would also like to acknowledge the financial support of the National Science Foundation (CBET-0933153), the Edward R. Weidlein Chair Professorship Funds and the Center for Complex Engineered Multifunctional Materials (CCEMM), Swanson School of Engineering at the University of Pittsburgh.

REFERENCES

- Shin JH, Hong SJ, Song HY, Park SJ, Ko GY, Lee SY, Kim HB, Jang JY. Placement of covered retrievable expandable metallic stents for pediatric tracheobronchial obstruction. *J Vasc Intervent Radiol* 2006;17(2 Pt 1):309–317.
- Maksoud-Filho JG, Goncalves ME, Cardoso SR, Tannuri U. Early diagnostic and endoscopic dilatation for the treatment of acquired upper airway stenosis after intubation in children. *J Pediatric Surg* 2008;43(7):1254–1258.
- Gallagher TO, Hartnick CJ. Tracheal resection and reanastomosis. *Adv Oto-Rhino-Laryngol* 2012;73:50–57.
- Xu X, Li D, Zhao S, Liu X, Feng Z, Ding H. Treatment of congenital tracheal stenosis by balloon-expandable metallic stents in paediatric intensive care unit. *Interact Cardiovasc Thorac Surg* 2012;14(5):548–550.
- Zaima A, Bitoh Y, Morita K, Tsugawa J, Ishii T, Satoh S, Nishijima E. Long-term T-tube stenting as definitive treatment of severe acquired subglottic stenosis in children. *J Pediatric Surg* 2010;45(5):996–999.
- Anton-Pacheco JL, Cabezali D, Tejedor R, Lopez M, Luna C, Comas JV, de Miguel E. The role of airway stenting in pediatric tracheobronchial obstruction. *Eur J Cardio-Thorac Surg* 2008;33(6):1069–1075.
- Preciado D, Zalzal G. Laryngeal and tracheal stents in children. *Curr Opin Otolaryngol Head Neck Surg* 2008;16(1):83–85.
- Mainwaring RD, Shillingford M, Davies R, Koltai P, Navaratnam M, Reddy VM, Hanley FL. Surgical reconstruction of tracheal stenosis in conjunction with congenital heart defects. *Ann Thorac Surg* 2012;93(4):1266–1272. discussion 1272–3.
- Charokopos N, Foroulis CN, Rouska E, Sileli MN, Papadopoulos N, Papakonstantinou C. The management of post-intubation tracheal stenoses with self-expandable stents: early and long-term results in 11 cases. *Eur J Cardio-Thorac Surg* 2011;40(4):919–924.
- Brigger MT, Boseley ME. Management of tracheal stenosis. *Curr Opin Otolaryngol Head Neck Surg* 2012;20(496):491–496.
- Nicolai T. Airway stents in children. *Pediatr Pulmonol* 2008;43(4):330–344.
- Mitsuoka M, Sakuragi T, Itoh T. Clinical benefits and complications of Dumon stent insertion for the treatment of severe central airway stenosis or airway fistula. *Gen Thorac Cardiovasc Surg* 2007;55(7):275–280.
- Mroz RM, Kordecki K, Kozlowski MD, Baniukiewicz A, Lewszuk A, Bondyra Z, Laudanski J, Dabrowski A, Chyczevska E. Severe respiratory distress caused by central airway obstruction treated with self-expandable metallic stents. *J Physiol Pharmacol* 2008;59(Suppl 6):491–497.
- Moravej M, Mantovani D. Biodegradable metals for cardiovascular stent application: Interests and new opportunities. *Int J Mol Sci* 2011;12(7):4250–4270.
- Kannan MB, Raman RKS. Evaluating the stress corrosion cracking susceptibility of Mg-Al-Zn alloy in modified-simulated body fluid for orthopaedic implant application. *Scripta Mater* 2008;59(2):175–178.
- Witte F, Fischer J, Beckmann F, Stoermer M, Hort N. Three-dimensional microstructural analysis of Mg-Al-Zn alloys by synchrotron-radiation-based microtomography. *Scripta Mater* 2008;58(6):453–456.
- Haenzi AC, Gerber I, Schinhammer M, Loeffler JF, Uggowitzer PJ. On the in vitro and in vivo degradation performance and biological response of new biodegradable Mg-Y-Zn alloys. *Acta Biomater* 2010;6(5):1824–1833.
- Li Z, Gu X, Lou S, Zheng Y. The development of binary Mg-Ca alloys for use as biodegradable materials within bone. *Biomaterials* 2008;29(10):1329–1344.
- Kannan MB, Raman RKS. In vitro degradation and mechanical integrity of calcium-containing magnesium alloys in modified-simulated body fluid. *Biomaterials* 2008;29(15):2306–2314.
- Chen Y, Yan J, Wang Z, Yu S, Wang X, Yuan Z, Zhang X, Zhao C, Zheng Q. In vitro and in vivo corrosion measurements of Mg-6Zn alloys in the bile. *Mater Sci Eng C-Mater Biol Appl* 2014;42:116–123.
- Qin H, Zhao Y, An Z, Cheng M, Wang Q, Cheng T, Wang Q, Wang J, Jiang Y, Zhang X, Yuan G. Enhanced antibacterial properties, biocompatibility, and corrosion resistance of degradable Mg-Nd-Zn-Zr alloy. *Biomaterials* 2015;53(0):211–220.
- Luffy SA, Chou DT, Waterman J, Wearden PD, Kumta PN, Gilbert TW. Evaluation of magnesium-yttrium alloy as an extraluminal tracheal stent. *J Biomed Mater Res Part A* 2014;102(3):611–620.
- Scheideler L, Fueger C, Schille C, Rupp F, Wendel HP, Hort N, Reichel HP, Geis-Gerstorfer J. Comparison of different in vitro tests for biocompatibility screening of mg alloys. *Acta Biomater* 2013;9(10):8740–8745.
- Marques MR, Loebenber R, Almukainzi M. Simulated biological fluids with possible application in dissolution testing. *Dissolution Technol* 2011;18(3):15–28.
- Witte F, Fischer J, Nellesen J, Crostack H-A, Kaese V, Pisch A, Beckmann F, Windhagen H. In vitro and in vivo corrosion measurements of magnesium alloys. *Biomaterials* 2006;27(7):1013–1018.